Robert E. Hogan, MD
Kevin E. Mark, DSc
Lei Wang, PhD
Sarang Joshi, PhD
Michael I. Miller, PhD
Richard D. Bucholz, MD

Index terms:
Brain, volume, 1341.839
Epilepsy
Hippocampus, 1341.92
Magnetic resonance (MR), image processing, 1341.121412
Magnetic resonance (MR), volume measurement, 1341.12141
Schizophrenia

Radiology 2000; 216:291–297

Abbreviations:
A1 = automatic segmentation 1
A2 = automatic segmentation 2
M1 = manual segmentation 1
M2 = manual segmentation 1

[1] From the Department of Neurology (R.E.H.) and the Division of Neurosurgery (R.D.B.), Saint Louis University, 3635 Vista Ave, St Louis, MO 63110; IntellX, Broomfield, Colo (K.E.M., S.J., R.D.B.); the Department of Psychiatry, Washington University School of Medicine, St Louis, Mo (L.W.); and the Center for Imaging Science, Whiting School of Engineering, Johns Hopkins University, Baltimore, Md (M.I.M.). Received May 17, 1999; revision requested July 19; final revision received October 12; accepted October 26. **Address correspondence to** R.E.H. (e-mail: *hoganr2@slu.edu*).

Author contributions:
Guarantor of integrity of entire study, R.E.H.; study concepts, R.E.H.; study design, R.E.H., K.E.M.; definition of intellectual content, R.E.H., K.E.M., M.I.M., S.J.; literature research, R.E.H.; clinical studies, R.E.H., R.D.B.; data acquisition, R.E.H.; data analysis, R.E.H., K.E.M., L.W.; statistical analysis, K.E.M.; manuscript preparation, R.E.H., K.E.M., S.J.; manuscript editing, R.E.H.; manuscript review, R.E.H., K.E.M., R.D.B.

Mesial Temporal Sclerosis and Temporal Lobe Epilepsy: MR Imaging Deformation-based Segmentation of the Hippocampus in Five Patients[1]

In five patients with mesial temporal sclerosis, the authors verified the precision and reproducibility of hippocampal segmentations with deformation-based magnetic resonance (MR) imaging. The overall percentage overlap between automated segmentations was 92.8% (SD, 3.5%), between manual segmentations was 73.1% (SD, 9.5%), and between automated and manual segmentations was 74.8% (SD, 10.3%). Deformation-based hippocampal segmentations provided a precise method of hippocampal volume measurement in this patient population.

Hippocampal volumetric measurements based on magnetic resonance (MR) images are helpful in the diagnosis and treatment of patients with mesial temporal lobe epilepsy. In the clinical setting of history of epileptic seizure compatible with mesial temporal lobe epilepsy, a meaningful hippocampal volume asymmetry is predictive of mesial temporal sclerosis (1,2) and a favorable outcome after epilepsy surgery (3–7).

Past studies have used manual segmentation of the hippocampus on MR images to determine hippocampal volumes (8). Although the sensitivity for detecting hippocampal asymmetry of manual segmentation as compared with visual inspection is greater in a proportion of patients with mesial temporal lobe epilepsy (9,10), manual segmentation is time-consuming and requires expertise in the details of hippocampal anatomy for accurate segmentations. The difficulty in manual segmentations lies in the subjective interpretations of anatomic variations. The emerging field of computational anatomy founded on general pattern theory (11) provides tools and a framework for accommodating and studying this variability (12–14). In this framework, an electronic atlas of the hippocampus is used as a deformable template that is matched to an individual MR image to extract and study the individual hippocampal areas.

Haller et al (15,16) describe a deformation-based hippocampal segmentation technique and verify the precision of this technique in healthy and schizophrenic patients. In this study, we evaluated the precision and reproducibility of deformation-based hippocampal segmentations in a group of patients with confirmed mesial temporal lobe epilepsy and mesial temporal sclerosis, which result in noteworthy changes in the size and shape (17) of the hippocampus.

Materials and Methods

MR imaging was performed with a 1.5-T imager (Signa; GE Medical Systems, Milwaukee, Wis). Whole-brain imaging was performed in the coronal plane with a fast spoiled gradient-recalled technique: repetition time msec/echo time msec of 14/3, flip angle of 30°, voxel dimensions of 0.859 × 0.859 × 1.5 mm, field of view of 22 × 22 cm, matrix size of 256 × 256.

Five patients (three men and two women) with refractory epilepsy were evaluated with MR imaging. Epilepsy in all patients had been refractory to multiple pharmacologic treatments. Mean duration of epilepsy at the time of epilepsy surgery was 9.4 years (range, 4.6–15.4 years). Mean age at the time of epilepsy

TABLE 1
Comparison of Percentage Overlap of Voxels between Segmentations

Hippocampal Segments	A1 vs A2	M1 vs M2	A1 vs M1
1R	96.5	78.9	77.9
2L	87.0	77.2	80.6
3R	96.3	85.4	82.4
4L	91.0	76.4	84.2
5R	96.6	86.0	89.6
1L	93.9	58.9	72.1
2R	94.6	72.4	66.5
3L	92.3	66.1	75.3
4R	92.0	69.7	62.5
5L	87.8	60.1	56.7
Normal hippocampi			
Mean	93.5	80.8	82.9
SD	4.3	4.6	4.4
Sclerotic hippocampi			
Mean	92.1	65.4	66.6
SD	2.6	5.9	7.4
Overall			
Mean	92.8	73.1	74.8
SD	3.5	9.5	10.3

Note.—Data are percentages. 1R, 2L, 3R, 4L, 5R, 1L, 2R, 3L, 4R, and 5L refer to patient number and right or left hippocampus.

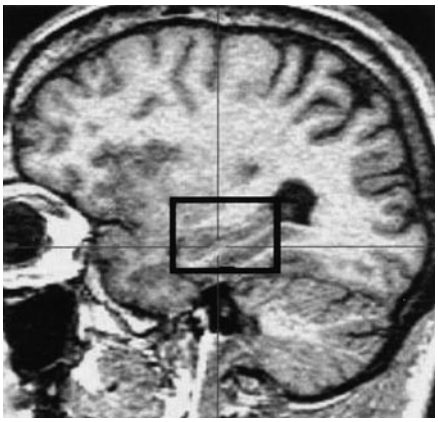

a.

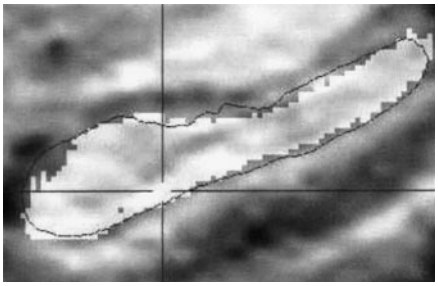

b.

Figure 1. Patient 2. **(a)** Sagittal fast spoiled gradient-recalled MR image (14/3, flip angle of 30°) through the left hippocampus. The region of interest is outlined in black. **(b)** The region of interest outlined in **a** is superimposed with manual (white shading) and deformation-based (gray outline) segmentations. (Original magnification, ×4.)

surgery was 32.2 years (range, 25–39 years). All patients were seizure free after epilepsy surgery (mean postoperative follow-up, 23.7 months; range, 18–33 months), and mesial temporal sclerosis was confirmed at postsurgical pathologic examination.

For manual hippocampal segmentation, MR images were integrated into an independent computer workstation and analyzed with software (ANALYZE AVW, version 1.1; Biomedical Imaging Resource, Mayo Foundation, Rochester, Minn). MR images were converted to an isotropic voxel dimension of 0.859. Intensities on these images were then adjusted to match those on the atlas image. For each image, a region of interest ($40 \times 40 \times 64$) was outlined for each hippocampus. This region of interest was converted to a voxel size of 0.4295 by means of interpolation, and final dimensions were $80 \times 80 \times 128$.

Two investigators (R.E.H., L.W.) independently segmented the hippocampi. Figure 1 shows general orientation of the MR image with respect to the outline of the region of interest. The hippocampi were segmented on the basis of anatomic boundaries described by Watson et al (18), with some exceptions. Watson et al used only coronal sections in their hippocampal tracings. We examined and segmented the hippocampus in coronal, sagittal, and transverse planes; we reviewed segmentations in each plane twice to ensure accurate tracings in all three dimensions. In Tables 1 and 2, patients' hippocampal images were referred to as 1R (patient 1, right hippocampal image), 1L (patient 1, left hippocampal image), and so on.

Instead of using the coronal section, which shows separation of the crus of the fornix from the hippocampal tail as the posterior border of the hippocampus, we included the entire hippocampal tail in our segmentations. We included the subiculum and excluded the alveus and fimbria (if visible) in our segmentations. The inferior margin of the subiculum was determined in the coronal plane of the body of the hippocampus by extending a straight horizontal line from the inferior border of the cornu ammonis and subiculum across the cortex of the parahippocampal gyrus. Cortex above this line was considered subiculum and that below this line was considered parahippocampal gyrus. Initial segmentation of the hippocampal head was performed in the coronal plane. If the uncal recess of the lateral ventricle or the alveus was visible, it was used in defining the superior border of the anterior part of the hippocampal head. If it was not visible, an initial approximation of the anterosuperior border of the hippocampal head was made by drawing a line from the inferior horn of the lateral ventricle to the inferior margin of the semilunar gyrus of the amygdala.

Verification of hippocampal head regions in the sagittal and transverse planes was often useful. In the sagittal plane, the medial aspect of the uncinate gyrus, the most medial part of the hippocampal head, was identified in the plane where the medial margin of the infolding of the uncal cleft was present inferiorly, and the semilunar gyrus was present superiorly (19). The semilunar gyrus often was present as a protuberance in the superior aspect of the amygdalohippocampal complex in this plane. Progressing from this plane laterally, the outline of the anterosuperior boundary of the hippocampal head was again verified in relationship to the uncal recess of the lateral ventricle and the alveus. The uncal cleft and subiculum were included in the inferior region of the segmentations. The transverse plane was often useful in defining the anterolateral region of the hippocampal head in relation to the lateral ventricle. Figure 2 is an image where the alveus is visible in the region of the hippocampal head. Figure 3 illustrates the use of landmarks to help define the hippocampal head when the alveus or the uncal recess of the lateral ventricle is not visible. Time for manual segmentation was approximately 2 hours per hippocampus.

TABLE 2
Volume Measurements and Hippocampal Volume Differences between Methods

Hippocampal Segments*	Automatic Segmentation			Manual Segmentation			Percentage Difference between Methods
	A1 Volume (mm^3)	A2 Volume (mm^3)	Absolute Percentage Difference	M1 Volume (mm^3)	M2 Volume (mm^3)	Absolute Percentage Difference	
1R	2,622	2,765	5.5	2,512	2,397	4.6	4.4
2L	2,592	2,429	6.3	2,792	2,513	10.0	7.2
3R	3,240	3,423	5.6	2,984	3,349	12.2	8.6
4L	2,306	2,224	3.6	2,433	2,494	2.5	5.2
5R	2,863	2,908	1.6	2,704	3,324	22.9	5.9
1L	1,537	1,687	9.8	1,880	1,294	31.2	18.2
2R	1,696	1,741	2.7	1,431	1,387	3.1	18.5
3L	1,307	1,292	1.1	1,605	1,239	22.8	18.6
4R	1,683	1,763	4.8	1,427	1,430	0.2	17.9
5L	1,553	1,527	1.7	1,646	1,256	23.7	5.7
Normal hippocampi							
Mean	2,725	2,750	4.5	2,685	2,815	10.4	6.2
SD	349	463	1.9	221	478	8.0	1.7
Sclerotic hippocampi							
Mean	1,555	1,602	4.0	1,598	1,321	16.2	15.8
SD	157	196	3.5	186	84	13.7	5.7
Overall							
Mean	2,140	2,176	4.3	2,141	2,068	13.3	11.0
SD	667	692	2.7	604	851	11.0	6.4

* 1R, 2L, 3R, 4L, 5R, 1L, 2R, 3L, 4R, and 5L refer to patient number and right or left hippocampus.

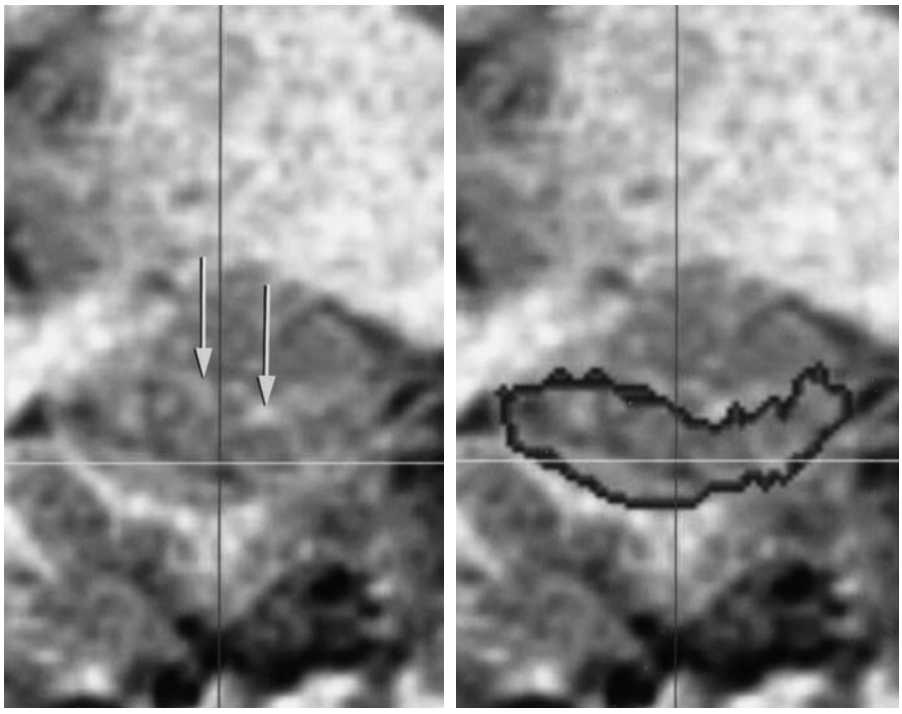

a. **b.**

Figure 2. Patient 3. **(a)** Coronal fast spoiled gradient-recalled MR image (14/3, flip angle of 30°) through the head of the right hippocampus. The alveus (arrows) is visible, especially in the mesial aspect of the hippocampal-amygdaloid complex. **(b)** The same section as in **a**, with superimposed manual segmentation (black outline) of the hippocampus. The alveus was excluded from the segmentation. In this example, the alveus was visible and therefore helped define the superior border of the hippocampal head in this region.

For deformation-based segmentations, MR data sets underwent preprocessing in preparation for the mapping algorithm. This consisted of two steps: determination of, first, global landmarks and, then, hippocampus-specific landmarks. Preprocessing was performed manually by means of Java-based software and took approximately 10–15 minutes per image.

Determination of landmarks provided an initial condition for the intensity-matching algorithm by roughly aligning the patient and atlas images. The first step in determining landmarks was identification of global landmarks, which scale and align the atlas brain to the patient brain on the basis of standard landmarks from the coordinate system of Talairach and Tournoux (20). The second step was individual determination of landmarks on each hippocampus. This was done by first identifying the head and tail of the hippocampus, which specifies the long axis of the hippocampus. Then, four landmarks were identified on five cross sections equally spaced along this axis. Landmarks were placed on the medial, lateral, superior, and inferior borders of the hippocampus on each cross section.

Images and landmark data were then integrated into a Unix-based software program. Within this program, the mapping algorithm used a coarse-to-fine procedure for generating a transformation field from an atlas reference MR image to a patient MR image. The atlas reference MR image was segmented as previously described (16). The coarse aspect of the procedure relied on the landmark information provided by expert segmenters to provide an

initial low-dimensional coregistration of atlas and patient images (21). The landmark information was provided in the form of the global and hippocampus-specific landmarks, which were used to derive a coarse manifold transformation (22) from the reference to the patient images.

After the coarse first step in the transformation was completed, the volumes were roughly aligned and attention was focused on the fine-featured substructures. The fine procedure involved the next two steps. The second step was to solve the registration problem by means of a linear elastic basis formulation and the full-volume data, as previously described (13,23). This was fully automatic and driven by only the volume data itself. The three-dimensional whole-brain maps corresponded to the maximizer, whose variation solution corresponded to a solution of a nonlinear partial differential equation, consisting of between 10^7 and 10^8 parameters. The third and final step of the algorithm was to solve the nonlinear partial differential equation corresponding to the Bayesian maximizer associated with the fluid formulation at each voxel of the full volume (12,24,25).

For the deformation-based segmentations, each data set was completely preprocessed (adjustment of intensity and determination of landmarks) twice at an interval of 2 months and run through the deformation-based algorithm.

Comparisons between two segmentations were made by computing the percentage overlap of voxels (Figs 4, 5). One segmentation was designated the reference (*R*) and the other the study (*S*) segmentation that we compared against the reference. The percentage overlap was computed as the number of overlapping segmented voxels between the two segmentations divided by the total number of segmented voxels in the study, that is, (*R* intersect *S*)/*S* × 100. We used the manual segmentations as the reference segmentations. Because a relatively larger or smaller reference image would effect the percentage overlap, automated segmentations were compared separately with the manual segmentations from both investigators. Between-group comparison of volume estimates was made by means of a paired Student *t* test (one tailed).

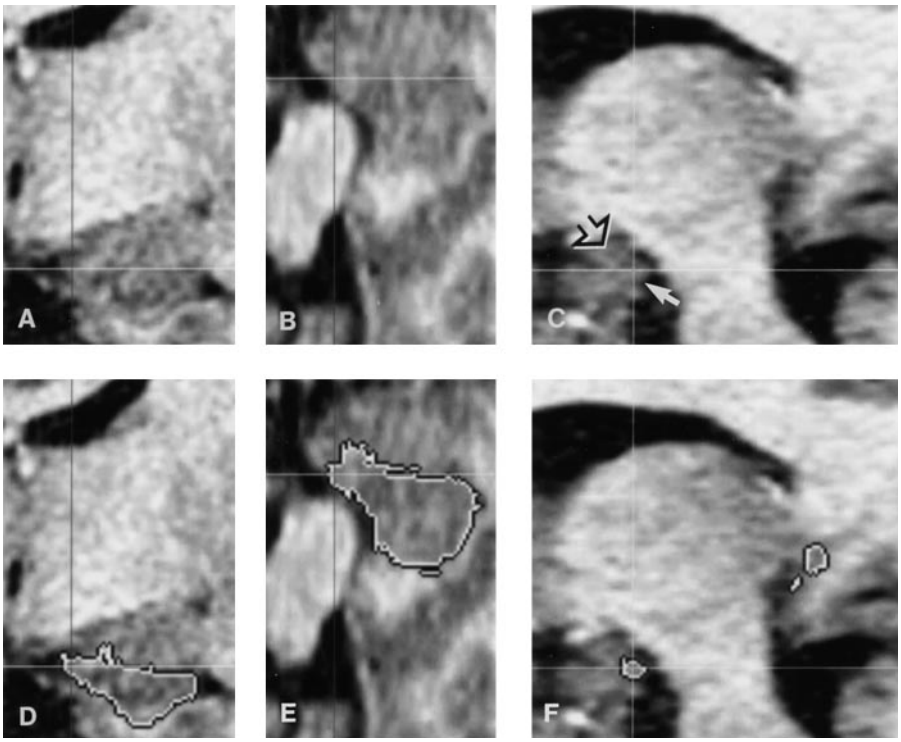

Figure 3. *A*, coronal; *B*, transverse; and *C*, sagittal fast spoiled gradient-recalled MR images (14/3, flip angle of 30°) illustrate the use of landmarks to help define the hippocampal head when the alveus or the uncal recess of the lateral ventricle is not visible. In *A–F*, crosshairs help orient the viewer to the mesial aspect of the uncinate gyrus of the hippocampus. In *C*, landmarks—the uncal cleft (solid arrow) and semilunar gyrus (open arrow) of the amygdala—help define the mesial extent of the hippocampus and differentiate it from the amygdala. The mesial aspect of the uncinate gyrus of the hippocampus lies adjacent to the superior margin of the uncal cleft in this plane. *D–F* are the same images as in *A–C*, respectively, with superimposed manual segmentations (black outline) of the hippocampus. *D* and *E* depict the anterior portion of the hippocampal head, and *F* depicts the most mesial extent of the hippocampal head (the uncinate gyrus, marked by crosshairs) and the tail of the hippocampus more posteriorly.

Results

Table 1 shows comparisons of four segmentations: two automatic segmentations (automatic segmentation 1 [A1] and automatic segmentation 2 [A2]) and two manual segmentations (manual segmentation 1 [M1] and manual segmentation 2 [M2]) performed by two experts in hippocampal anatomy (M1, R.E.H.; M2, L.W.).

The means and SDs of the percentage overlap were computed for three subsets of the data: normal hippocampi, sclerotic hippocampi, and all hippocampi. Overall comparisons showed a mean percentage overlap of 92.8% (SD, 3.5) between A1 and A2, 73.1% (SD, 9.5) between M1 and M2, and 74.8% (SD, 10.3) between A1 and M1. The relatively large percentage overlap between A1 and A2 demonstrates the reproducibility of the deformation-based segmentation procedure. The last two vales demonstrate that the automatic segmentation procedure performed comparably with manual segmentation.

The mean percentage overlap for the subset of normal hippocampi were 80.8% (SD, 4.6) between M1 and M2 and 82.9% (SD, 4.4) between A1 and M1. The mean percentage overlap for the subset of sclerotic hippocampi were 65.4% (SD, 5.9) between M1 and M2 and 66.6% (SD, 7.4) between A1 and M1. The decrease in mean percentage overlap between segmentation of normal versus sclerotic hippocampi reflects the increased ambiguity and difficulty in segmenting the sclerotic hippocampi.

Table 2 shows volume measurements based on the four segmentations. Mean values for absolute percentage differences for normal hippocampi were the following: A1 versus A2, 4.5% (SD, 1.9%); M1 versus M2, 10.4% (SD, 8.0%); A1 versus M1, 6.2% (SD, 1.7%). Mean values for absolute percentage differences for sclerotic hippocampi were the following: A1 versus A2, 4.0% (SD, 3.5%); M1 versus M2, 16.2% (SD, 13.7%); A1 versus M1, 15.8% (SD, 5.7%). Mean values for absolute percentage differences for all hippocampi were the following: A1 versus A2, 4.3% (SD, 2.7%); M1 versus M2, 13.3% (SD, 11.0%); A1 versus M1, 11.0% (SD, 6.4%). Results of volume comparisons

Figure 4. Patient 1. Sagittal representations of segmentations with 6-mm section thickness in a normal hippocampus illustrate the overlap of manual (gray areas) and deformation-based (white outlines) segmentations of the right hippocampus. The margins of the structures show the most differences.

also showed greater differences in the sclerotic hippocampi.

Finally, comparisons of percentage overlap, considering all hippocampi, were calculated with use of either M1 or M2 as the reference. The comparisons to M1 as the reference showed that the automatic segmentations had a mean percentage overlap of 74.8% (M1 vs A1) and 78.5% (M1 vs A2) as compared with 73.1% (M1 vs M2). Similarly, with M2 as the reference, the mean percentage overlap of A1 (M2 vs A1) was 74.9% and the of A2 (M2 vs A2) was 76.9%.

Discussion

Hippocampal volumetric measurements have many clinical applications, including the diagnosis and treatment of mesial temporal lobe epilepsy. Clinical applications in temporal lobe epilepsy include favorable localization value when compared with results from scalp and intracranial electroencephalography (2), correlation with neuropsychologic evaluation (26), and prediction of favorable outcome after temporal lobectomy for intractable mesial temporal lobe epileptic seizures (8). These important clinical applications were recently thoroughly reviewed by Watson et al (8).

Past techniques measuring the hippocampus have focused on defining structures in a single two-dimensional plane. There are advantages of measuring the hippocampus in the coronal plane, which is perpendicular to the long axis of the hippocampal body (18). Certain hippocampal structures, such as the boundary between the subiculum and parahippocampal gyrus in the body of the hippocampus, are most easily identifiable in the coronal plane. Because of the three-dimensional shape of the hippocampus, however, especially the hippocampal head, which turns medially and superiorly in relationship to the hippocampal body, we have found advantages in verifying hippocampal segmentations in coronal, sagittal, and transverse planes. Because the boundaries of the hippocampal head were the most difficult to define, verification of three-dimensional relationships in this region was most helpful. The indistinct boundary between the uncinate gyrus of the hippocampus and ambient gyrus of the amygdala was often best determined by using landmarks in the sagittal plane, as described in Materials and Methods. Figure 3 illustrates this region. Other investigators have commented on the advantages of segmentation of the hippocampal head region by means of three-dimensional segmentations (27,28).

Our results show reproducibility and are comparable to those in past studies. Direct comparison with past validation studies is difficult, however, owing to differences in acquisition parameters of images in different studies (27), past documentation of validation in only healthy subjects (29), and differences in anatomic boundaries and segmentation techniques used for segmentations (8). These differences have produced a wide variation in normal hippocampal volumes in different studies (30).

Most past validation studies have used manual segmentation techniques (27–29). With use of general pattern matching, anatomic structures can be segmented on the basis of global shape models. By using templates that represent the typical structures, MR images of the hippocampus may be semiautomatically segmented by means of template transformations to define hippocampal variability (12,13,22). Haller et al (15) reported a method of hippocampal segmentation based on general pattern matching. In a comparison of two-dimensional measurements of a segment of the hippocampus on the basis of general pattern matching, the mean difference between two segmentations was 1.33%, while that between two manual segmentations was 4.67%.

Our validation is most comparable to that performed by Haller et al (16), in which investigators validated a deformation hippocampal segmentation technique by comparing control subjects and patients with schizophrenia. They performed two deformation and two manual segmentations on MR images of the right hippocampus in five healthy and five schizophrenic patients. The mean percentage difference between absolute volumes for automatic and manual segmentations, respectively, were 3.6% and 4.2% for healthy subjects and 2.5% and 10.1% for schizophrenic patients. Between-method mean percentage differences in volumes (with use of nonabsolute values) for automated versus manual segmentations were −0.7% (range, 6.4% to −12.2%; SD, 7.0%) for healthy subjects and −2.4% (range, 14.1% to −11.1%; SD, 10.6%) for schizophrenic patients. Overall percentage overlap (considering both healthy and schizophrenic groups together) between automated segmentations was 91.4% (SD, 3.6%), between manual segmentations was 77.9% (SD, 4.8%), and between automated and manual segmentations was 74.2% (SD, 5.5%). The between-method percentage differences for absolute volumes and overall percentage overlap were calculated in a similar manner in our study and the study of Haller et al (16). Our results for differences in absolute percentage volume and percentage overlap were comparable. In a comparison of automated versus manual segmentations, our between-method absolute percentage differences in volumes were 6.2% (range, 4.4%–8.6%; SD, 1.7%) for normal hippocampi and 15.8% (range, 5.7%–18.6%; SD, 5.7%) for sclerotic hippocampi. Our values for overall percentage overlap between automated segmentations were 92.8% (SD, 3.5%), between manual segmentations was 73.1% (SD, 9.5%), and between automated and manual segmentations was 74.8% (SD, 10.3%). Differences in percentage overlap and percentage volume were similar between the manual segmentations and the automated versus manual segmentations, demonstrating a similar variability in the automatic and manual segmentations when compared with the same control.

In our study, as in the study by Haller et al (16), results in normal hippocampi were in better concordance than were those in abnormal hippocampi with both automated and manual segmentations. Past studies have shown greater percentage error when segmentations involve smaller volumes (31). In a study of progressive multiple sclerosis lesions de-

picted at MR imaging, Goodkin et al (31) found a coefficient of variation for three successive lesion measurements that was inversely related to the lesion area and ranged from 22.6% for lesions smaller than 0.67 cm^2 to 12.1% for larger lesions. Past authors have used logarithmic comparisons to account for percentage volume differences in structures that are of different size (28). Therefore, greater variance could be expected in the segmentation of sclerotic hippocampi because they are smaller than normal hippocampi.

Another possible source of error is that deformation mapping of the normal hippocampus onto an atrophic hippocampus may be slightly more difficult for the mapping algorithm than is mapping onto a normal hippocampus. This could possibly increase variability in deformation segmentations of sclerotic hippocampi. Determination of landmarks is also variable in automated segmentations and is also more difficult in atrophic hippocampi. Our results indicate increased difficulty in defining hippocampal borders with either the deformation or manual segmentation technique when the hippocampus is small or abnormally shaped.

A comparison of percentage overlap of voxels with use of either M1 or M2 as the reference did not show appreciable differences. Given the formula for calculating percentage overlap, a relatively larger reference would produce a higher percentage overlap, and a relatively smaller reference would produce a relatively lower percentage overlap. The comparable values of percentage overlap calculated with either M1 or M2 as a reference indicate that the size of M1 and M2 is comparable. This was confirmed in the comparisons of volume.

There are many clinical applications for MR-based hippocampal volumetric studies. Many studies continue to explore applications in the areas of epilepsy, Alzheimer disease (32,33), amnesic syndromes (34), and schizophrenia (35,36). We demonstrated that our deformation-based segmentation technique produces reliable segmentation of the hippocampi in patients with mesial temporal sclerosis and mesial temporal lobe epilepsy. Practically, this semiautomated technique allows segmentation of both hippocampi in approximately 10–15 minutes of user time, which is shorter than the time needed to produce accurate segmentations with manual segmentation—approximately 2 hours per hippocampus in this study. Other investigators performing segmentation with images of different voxel sizes report taking approximately 40 minutes per hippocampus (27).

Figure 5. Patient 3. Sagittal representations of segmentations with 4-mm section thickness in a sclerotic hippocampus illustrate the overlap of manual (gray areas) and deformation-based (white outlines) segmentations of the left hippocampus. As in Figure 4, the margins of the structures show greater segmentation differences. In comparison with Figure 4, however, the differences are more accentuated in the region of the uncinate gyrus (arrow). This segmentation difference is likely due to the lack of distinct anatomic boundaries in this region of the hippocampus, coupled with the anatomic changes that accompany mesial temporal sclerosis.

Deformation-based segmentation can help examine three-dimensional aspects of hippocampal shape. Analysis of changes in shape of schizophrenic versus normal hippocampi showed changes, but volume changes alone were not different (21,35,37). Analysis of hippocampal shape may also have important applications in the diagnosis of other central nervous system disorders. Shape analysis enables evaluation of local details of hippocampal anatomy that may not be evident in measurements of total hippocampal volume (Fig 6). In epilepsy, hippocampal sclerosis may be present without associated asymmetry in total hippocampal volume (38). There are also well-documented changes in regional hippocampal anatomy, such as volume loss localized to only the hippocampal head (17,39) or

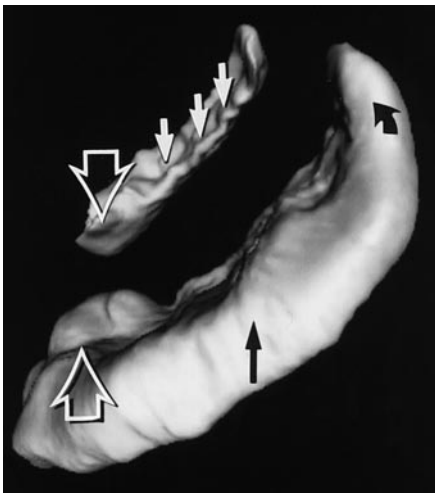

Figure 6. Lateral three-dimensional deformation-based surface-rendered images provide a perspective that assists visual inspection of the segments of the hippocampus. In the more distant hippocampus, the subiculum (solid arrows) and mesial aspects of the hippocampal head (open arrow) are clearly depicted. In the near hippocampus, the head (open arrow), body (solid straight arrow), and tail (curved arrow) of the hippocampus are depicted.

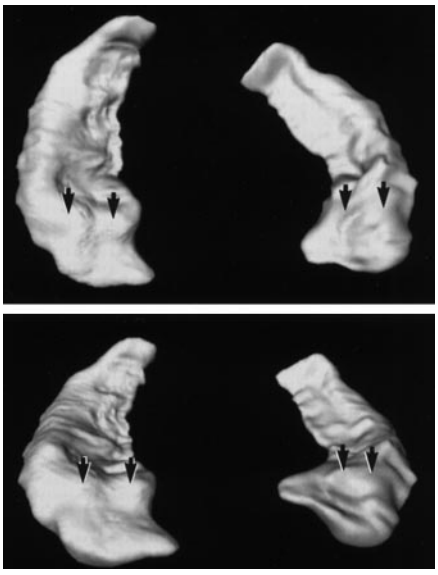

Figure 7. Patient 1. Three-dimensional surface-rendered images of the hippocampi from above (top) and an anterior vantage point (bottom). Digitations (arrows) of the hippocampal head (pes hippocampi) are visible in the normal (right) hippocampi but are not visible in the sclerotic (left) hippocampi.

loss of digitations of the hippocampal head (40). For the latter in MR diagnosis of mesial temporal sclerosis, sensitivity was 92% and specificity was 100%. Figure 7 illustrates the way deformation-based

segmentations can highlight structural changes in the hippocampal head. Application of deformation shape analysis may enable better localization of neuroanatomic abnormalities in patients with mesial temporal lobe epilepsy.

Acknowledgment: The authors thank John G. Csernansky, MD, for his contributions to development of the hippocampal segmentation used as the atlas template for the deformation-based segmentations.

References

1. Lencz T, McCarthy G, Bronen RA, et al. Quantitative magnetic resonance imaging in temporal lobe epilepsy: relationship to neuropathology and neuropsychological function. Ann Neurol 1992; 31:629–637.
2. Cascino GD. Clinical correlations with hippocampal atrophy. Magn Reson Imaging 1995; 13:1133–1136.
3. Jack CR Jr, Sharbrough FW, Cascino GD, Hirschorn KA, O'Brien PC, Marsh WR. Magnetic resonance image-based hippocampal volumetry: correlation with outcome after temporal lobectomy. Ann Neurol 1992; 31:138–146.
4. Cascino GD. Clinical evaluation and noninvasive electroencephalography: preoperative evaluation. Neuroimaging Clin N Am 1995; 5:547–558.
5. Kim JH, Tien RD, Felsberg GJ, Osumi AK, Lee N, Friedman AH. Fast spin-echo MR in hippocampal sclerosis: correlation with pathology and surgery. AJNR Am J Neuroradiol 1995; 16:627–636.
6. Arruda F, Cendes F, Andermann F, et al. Mesial atrophy and outcome after amygdalohippocampectomy or temporal lobe removal. Ann Neurol 1996; 40:446–450.
7. Holmes MD, Dodrill CB, Ojemann GA, Wilensky AJ, Ojemann LM. Outcome following surgery in patients with bitemporal interictal epileptiform patterns. Neurology 1997; 48:1037–1040.
8. Watson C, Jack CR Jr, Cendes F. Volumetric magnetic resonance imaging: clinical applications and contributions to the understanding of temporal lobe epilepsy. Arch Neurol 1997; 54:1521–1531.
9. Cendes F, Leproux F, Melanson D, et al. MRI of amygdala and hippocampus in temporal lobe epilepsy. J Comput Assist Tomogr 1993; 17:206–210.
10. Reutens D, Cook M, Kingsley D, et al. Volumetric MRI is essential for reliable detection of hippocampal asymmetry (abstr). Epilepsia 1993; 34:138.
11. Grenander U. General pattern theory. London, England: Oxford University Press, 1993.
12. Christensen GE, Rabbitt RD, Miller MI. A deformable neuroanatomy textbook based on viscous fluid mechanics. In: Prince J, Runolfsson T, eds. Proceedings of the 27th Annual Conference on Information Sciences and Systems. Baltimore, Md: the Johns Hopkins University, 1993; 211–216.
13. Miller MI, Christensen GE, Amit Y, Grenander U. Mathematical textbook for deformable neuroanatomies. Proc Natl Acad Sci U S A 1993; 90:11944–11948.
14. Miller MI, Grenander U. Computational anatomy: an emerging discipline. Q Appl Math 1998; 5:617–694.
15. Haller JW, Christensen GE, Joshi SC, et al. Hippocampal MR imaging morphometry by means of general pattern matching. Radiology 1996; 199:787–791.
16. Haller JW, Banerjee A, Christensen GE, et al. Three-dimensional hippocampal MR morphometry with high-dimensional transformation of a neuroanatomic atlas. Radiology 1997; 202:504–510.
17. Cook MJ, Fish DR, Shorvon SD, Straughan K, Stevens JM. Hippocampal volumetric and morphometric studies in frontal and temporal lobe epilepsy. Brain 1992; 115: 1001–1015.
18. Watson C, Andermann F, Gloor P, et al. Anatomic basis of amygdaloid and hippocampal volume measurement by magnetic resonance imaging. Neurology 1992; 42:1743–1750.
19. Duvernoy HM. The human hippocampus: an atlas of applied anatomy. New York, NY: Springer-Verlag, 1988; 98–125.
20. Talairach J, Tournoux P. Coplanar sterotactic atlas of the human brain. New York, NY: Thieme, 1988.
21. Joshi S. Large deformation diffeomorphisms and gaussian random fields for statistical characterization of brain submanifolds. Dissertation. Washington University, Saint Louis, Mo, 1997.
22. Joshi SC, Miller MI, Christensen GE, Banerjee A, Coogan TA, Grenander U. Hierarchical brain mapping via a generalized Dirichlet solution for mapping brain manifolds. Proc SPIE Inter Symp Opt Sci Eng Instrum 1995; 2573:278–289.
23. Christensen GE, Rabbitt RD, Miller MI. (3D) Brain mapping using a deformable neuroanatomy. Phys Med Biol 1994; 39: 609–618.
24. Christensen GE, Rabbitt RD, Miller MI, Joshi SC, Grenander U, Coogan TA. Topological properties of smooth anatomic maps. In: Bizais Y, Barillot C, DiPaola R, eds. Information processing in medical imaging. Norwell, Mass: Kluwer Academic, 1995; 101–112.
25. Christensen GE, Joshi SC, Miller MI. Volumetric transformation of brain anatomy. IEEE Trans Med Imaging 1997; 16:864–877.
26. Baxendale SA, Van Paesschen W, Thompson PJ, Duncan JS, Shorvon SD, Connelly A. The relation between quantitative MRI measures of hippocampal structure and the intracarotid amobarbital test. Epilepsia 1997; 38:998–1007.
27. Hasboun D, Chantome M, Zouaoui A, et al. MR determination of hippocampal volume: comparison of three methods. AJNR Am J Neuroradiol 1996; 17:1091–1098.
28. Bartzokis G, Altshuler LL, Greider T, Curran J, Keen B, Dixon WJ. Reliability of medial temporal lobe volume measurements using reformatted 3D images. Psychiatry Res 1998; 82:11–24.
29. Jack CR Jr, Bentley MD, Twomey CK, Zinsmeister AR. MR imaging-based volume measurements of the hippocampal formation and anterior temporal lobe: validation studies. Radiology 1990; 176: 205–209.
30. Jack CR, Theodore WH, Cook M, McCarthy G. MRI-based hippocampal volumetrics: data acquisition, normal ranges, and optimal protocol. Magn Reson Imaging 1995; 13:1057–1064.
31. Goodkin DE, Ross JS, Medendorp SV, Konecsni J, Rudick RA. Magnetic resonance imaging lesion enlargement in multiple sclerosis: disease-related activity, chance occurrence, or measurement artifact? Arch Neurol 1992; 49:261–263.
32. Jack CR Jr, Petersen RC, Xu Y, et al. Rate of medial temporal lobe atrophy in typical aging and Alzheimer's disease. Neurology 1998; 51:993–999.
33. Frisoni GB, Laakso MP, Beltramello A, et al. Hippocampal and entorinhal cortex atrophy in frontotemporal dementia and Alzheimer's disease. Neurology 1999; 52: 91–100.
34. Press GA, Amaral DG, Squire LR. Hippocampal abnormalities in amnesic patients revealed by high-resolution magnetic resonance imaging. Nature 1989; 341:54–57.
35. Csernansky JG, Joshi S, Wang L, et al. Hippocampal morphometry in schizophrenia by high dimensional brain mapping. Proc Natl Acad Sci U S A 1998; 95:11406–11411.
36. Shenton ME, Kikinis R, Jolesz FA, et al. Abnormalities of the left temporal lobe and thought disorder in schizophrenia: a quantitative magnetic resonance imaging study. N Eng J Med 1992; 327:604–612.
37. Joshi S, Miller MI, Grenander U. On the geometry and shape of brain sub-manifolds (abstr). Int J Pattern Recognition Artificial Intell 1997; 11:8.
38. Jackson GD, Kuzniecky RI, Cascino GD. Hippocampal sclerosis without detectable hippocampal atrophy. Neurology 1994; 44:42–46.
39. Bronen RA, Fulbright RK, Kim JH, Spencer SS, Spencer DD, al-Rodhan NR. Regional distribution of MR findings in hippocampal sclerosis. AJNR Am J Neuroradiol 1995; 16:1193–1200.
40. Oppenheim C, Dormont D, Biondi A, et al. Loss of digitations of the hippocampal head on high-resolution fast spin-echo MR: a sign of mesial temporal sclerosis. AJNR Am J Neuroradiol 1998; 19:457–463.